Chapter 2
Experimental Technique and Working Modes

S. Sadewasser

Abstract Kelvin probe force microscopy is a scanning probe microscopy technique providing the capability to image the local surface potential of a sample with high spatial resolution. It is based on the non-contact atomic force microscope and minimizes the electrostatic interaction between the scanning tip and the surface. The two main working modes are the amplitude modulation and the frequency modulation mode, in which the electrostatic force or the electrostatic force gradient are minimized by the application of a dc bias voltage, respectively. For metals and semiconductors, the contact potential difference is determined, which is related to the sample's work function, while for insulators information about local charges is obtained. This chapter provides a brief introduction to non-contact atomic force microscopy and describes the details of the various Kelvin probe force microscopy techniques.

2.1 Introduction

Surface science was revolutionized in 1982 by the invention of the scanning tunneling microscope (STM) by Binnig and Rohrer [3]. In 1986 the invention of the atomic force microscope (AFM) widened the range of samples from conductive to non-conductive ones [4]. Further development led to the non-contact (or dynamical) mode of the AFM [20], where a cantilever supporting a sharp tip at its end is vibrated close to its resonance frequency and changes in the vibration due to tip-sample interaction are employed to maintain a constant distance to the sample surface while scanning across the sample. Forces exerted by the tip on the sample are minimal in non-contact mode.

S. Sadewasser (✉)
International Iberian Nanotechnology Laboratory - INL, Avda. Mestre José Veiga s/n, 4715-330 Braga, Portugal
e-mail: sascha.sadewasser@inl.int

S. Sadewasser and T. Glatzel (eds.), *Kelvin Probe Force Microscopy*, Springer Series in Surface Sciences 48, DOI 10.1007/978-3-642-22566-6_2,

A wide field of applications has been opened by the combination of the AFM with other measurement methods, thus providing additional sample properties on a lateral scale in the nanometer range. One representative, the Kelvin probe force microscope (KPFM) was first developed by Nonnenmacher et al. [23] and it allows to image surface electronic properties, namely the contact potential difference (CPD). The name "Kelvin probe force microscope" originates from the macroscopic method developed by Lord Kelvin in 1898 using a vibrating parallel plate capacitor arrangement, where a voltage applied to one vibrating plate is controlled such that no current is induced by the vibration [17]. The reduction of this exact principle to the microscopic scale however results in a poor sensitivity, since the size of the plates is too small to generate a sufficient current. Therefore, in KPFM the electrostatic force is used. The cantilever in an AFM is a very sensitive force sensor, thus the CPD can be measured with high sensitivity. A dc-bias applied to the sample (or the tip) is controlled in such a way that the electrostatic forces between tip and sample are minimized.

This chapter will initially describe the working principle of non-contact atomic force microscopy (nc-AFM) and then explain the KPFM technique. Two working modes will be described which are both widely applied in research laboratories. At the end of the chapter some notes on other working modes are given.

2.2 Non-Contact Atomic Force Microscopy

An AFM consists of a sharp tip supported at the end of a cantilever serving as a force sensor [4]. The sample's topography is imaged by scanning the tip across a sample surface while maintaining a constant force or force gradient by a feedback loop. Different modes for AFM operation can be used. In contact mode the tip is brought into contact with the sample, and repulsive tip-sample interaction is measured. In non-contact mode (also called dynamic mode) the tip is oscillated at or near its fundamental resonance frequency [20]. The oscillation is mechanically excited using a piezoelectric element on which the cantilever-chip is mounted. Interaction forces between tip and sample cause a shift in the resonance frequency. A third mode uses an oscillating cantilever, however, the regime of repulsive tip-sample interaction is reached in the lower turn-around point of the oscillation cycle, while in the rest of the oscillation cycle attractive forces act. In this tapping mode and in the non-contact mode the forces exerted by the scanning tip on the sample are considerably reduced with respect to the contact mode.

In nc-AFM the cantilever is oscillated at or near its resonance frequency and the change in the oscillation is monitored in dependence of the tip-sample interaction. Figure 2.1 shows the basic AFM experimental setup consisting of the cantilever and tip, the sample on a xyz-stage with piezo control, and the detection system with a laser and a position sensitive photo diode. Alternatively to the displayed beam-deflection detection an interferometric technique or a piezoelectric and piezoresistive detection can be used.

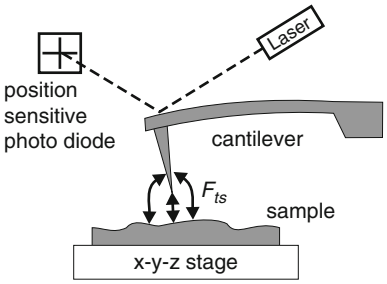

Fig. 2.1 Working principle of an AFM consisting of the beam deflection detection system with laser and position sensitive photo diode and the sample on a piezo-driven xyz-stage

The oscillation of the cantilever can be described by its equation of motion, which in general is a three dimensional problem. By considering the tip as a point-mass spring the equation of motion for the tip can be represented as [10]:

$$m\ddot{z} + \frac{m\omega_0}{Q}\dot{z} + kz = F_{\mathrm{ts}} + F_0 \cos(\omega_{\mathrm{d}} t), \tag{2.1}$$

where k denotes the spring constant, Q the quality factor, F_{ts} the tip-surface interaction, F_0 and ω_{d} the amplitude and angular frequency of the driving force, respectively. The free resonance frequency f_0 (without tip-surface interaction, $F_{\mathrm{ts}} = 0$) is a function of the spring constant k and the effective mass m^*, which also accounts for the specific geometry of the cantilever:

$$\omega_0 = 2\pi f_0 = \sqrt{\frac{k}{m^*}}. \tag{2.2}$$

When the tip is approached to the surface, forces act between tip and sample. This tip-surface interaction may consist of various contributions, short range repulsive and chemical binding forces, the van der Waals force F_{vdW}, and the long-range electrostatic and magnetic forces, F_{el} and F_{mag}, respectively. The short-range interaction is usually described by the empirical Lennard-Jones type interaction potential, which is illustrated in Fig. 2.2 [15]. The repulsive force can be described by a power law interaction potential:

$$U_{\mathrm{rep}} = \left(\frac{\sigma_0}{r}\right)^n, \tag{2.3}$$

where the exponent is usually set to $n = 12$. Frequently, this repulsive part is also described by an exponential dependence:

$$U_{\mathrm{rep}} = c \cdot \mathrm{e}^{-r/\sigma'}. \tag{2.4}$$

Here σ_0 and σ' are characteristic lengths, where σ' is on the order of 0.02 nm.

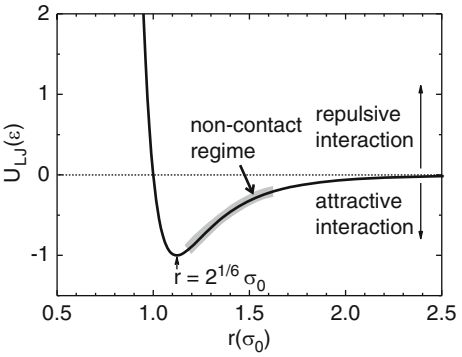

Fig. 2.2 Lennard-Jones type interaction potential describing the typical interaction of an AFM tip and the sample surface at small tip-sample distances

At larger distance, the interaction potential becomes attractive, goes through a minimum and then becomes smaller toward large tip-sample distances. The total short-range interatomic interaction potential comprising the repulsive and attractive part is thus described by a Lennard-Jones potential [15]:

$$U_{\mathrm{LJ}} = 4\epsilon \left[\left(\frac{\sigma_0}{r} \right)^{12} - \left(\frac{\sigma_0}{r} \right)^{6} \right], \tag{2.5}$$

as illustrated in Fig. 2.2.

The repulsive force at very small tip-sample distances results from the Pauli exclusion principle for the overlapping electron clouds of the tip and sample atoms. The chemical forces are due to the bonding state of a quantum mechanical overlap of the electron wave functions of tip and sample. These chemical interactions obey an exponential distance dependence and are only relevant at distances below ∼5 Å[24].

An additional contribution to the attractive part of the short-range interaction force is the van der Waals force. It is an always present interaction between atoms and molecules due to the interaction between induced electrostatic dipoles, i.e., as a result of electromagnetic field fluctuations. For the case of AFM, it can be approximated by considering a sphere of radius R in front of an infinite plane, representing the sample surface, and is usually expressed as [10, 15]:

$$F_{\mathrm{vdW}} = -\frac{HR}{6d^2}, \tag{2.6}$$

where H is the Hamaker constant, and d the closest distance between the sphere and the plane (the tip and the sample). For tip-sample distances smaller than an intermolecular distance a_0, F_{vdW} is replaced by the adhesion force F_{adh}. For the case of a stiff contact and a small tip radius the adhesion force can be described by $F_{\mathrm{adh}} = -4\pi R\gamma$, where γ is the surface energy [7, 10, 38]. As indicated by the

gray area of the interaction potential in Fig. 2.2, nc-AFM is operated in the attractive region of the interaction.

The relevant force for KPFM is the electrostatic force F_{el}. It can be expressed by considering the tip-sample system as a capacitor. Thus, with the energy of a capacitor, $U_{\mathrm{el}} = 1/2C\,V^2$, the force can be written as:

$$F_{\mathrm{el}} = -\nabla U_{\mathrm{el}} = -\frac{1}{2}\frac{\partial C}{\partial r}V^2 - C\,V\frac{\partial V}{\partial r}, \tag{2.7}$$

where C is the capacitance and V the total voltage. For simplicity, a metallic tip and sample can be considered. In the case of AFM, the most significant contribution is due to the forces perpendicular to the sample surface (denominated z-direction), therefore (2.7) simplifies to:

$$F_{\mathrm{el}} = -\frac{1}{2}\frac{\partial C}{\partial z}V^2. \tag{2.8}$$

A detailed discussion of the electrostatic force will follow in the next section. The magnetic forces are only relevant if tip and/or sample material are magnetic. Generally, for KPFM this is not the case and therefore these forces will not be considered here.

When approaching the tip to the sample, the interaction forces will cause a shift of the resonance curve of the cantilever. For small oscillation amplitudes the system can be regarded as a weakly perturbed harmonic oscillator. In this case the shift of the resonance curve can be approximated by introducing an effective spring constant k_{eff} [10]:

$$k_{\mathrm{eff}} = k - \frac{\partial F_{\mathrm{ts}}}{\partial z}. \tag{2.9}$$

The spring constant is lowered by the force gradient. For small force gradients this shifts the resonance curve, in the case of attractive forces to lower frequencies and vice versa. The frequency shift can be approximated by [2, 10]:

$$\Delta f_0 = -\frac{f_0}{2k}\frac{\partial F_{\mathrm{ts}}}{\partial z}. \tag{2.10}$$

Equation (2.9) and (2.10) are approximations to the solution of the equation of motion (2.1) for small oscillation amplitude and small force gradients. In many situations they provide a quick and easy way to interpret the experiments. However, in many practical cases of KPFM, large oscillation amplitudes are used, and thus throughout the oscillation cycle the tip-sample interaction continuously varies. The above approximations are no longer valid in this case and more elaborate methods have to be used. In classical first-order pertubation theory the solution to the equation of motion gives the frequency shift Δf_0 as a function of the tip-sample distance d, the oscillation amplitude A_0, the spring constant k and the free resonance frequency f_0 as [10, 11]:

$$\Delta f_0 = -\frac{f_0}{kA_0^2}\frac{1}{T_0}\int_0^{T_0} F_{\mathrm{ts}}\left(d + A_0 + A_0\cos(2\pi f_0 t)\right) A_0\cos(2\pi f_0 t)\,\mathrm{d}t. \quad (2.11)$$

Two different detection modes can be applied in nc-AFM. For the amplitude modulation technique (AM-mode) [20] the cantilever is excited at a constant frequency slightly off resonance. A change in the tip-sample distance leads to a change of the force gradient, which results in a shift of the resonance peak; thus, the oscillation amplitude at the fixed driving frequency changes. A feedback loop adjusts the tip-sample distance to maintain a constant amplitude. This detection method is usually applied in air, where the quality factor Q of the cantilever is on the order of 1–10^2. When operating a nc-AFM in vacuum, the quality factor increases by several orders of magnitude (typically above 10^5) due to the reduced damping. This results in a reduced band width for the detection and a very slow response time of the system is the consequence [2]. Albrecht et al. [2] have introduced the frequency modulation technique (FM-mode) for application in vacuum. In this mode, the change of the resonance curve is detected by directly measuring the frequency shift of the resonance curve. The cantilever serves as the frequency determining element and is excited at its resonance frequency using a positive feedback. Through an automatic gain control (AGC) the oscillation amplitude is kept constant. The resonance frequency is measured using a frequency demodulator, or a phase locked loop (PLL), for example. For a change of the tip-sample distance during the scan the resonance frequency changes and the z-controller adjusts the tip-sample distance to maintain a constant frequency shift Δf_0 with respect to the free resonance of the cantilever. The experimental set-up of this FM-mode is illustrated in Fig. 2.7 in Sect. 2.7 below. For both modes, according to (2.10), the measured surface topography approximately corresponds to a surface of constant force gradient.

2.3 Kelvin Probe Force Microscopy

The KPFM combines the nc-AFM with the Kelvin probe technique. The macroscopic Kelvin probe technique was developed in 1898 by Lord Kelvin [17] for the measurement of surface potentials: the sample constitutes one plate of a parallel plate capacitor, with a known metal forming the other plate, which is vibrated at frequency ω. Due to the changing distance between the plates, the capacitance changes, resulting in an alternating current in the circuit connecting the plates. This current is reduced to zero by applying a dc-voltage to one of the plates. This voltage corresponds to the CPD of the two materials.

The KPFM employs the same principle, applying a dc-voltage to compensate the CPD between the AFM tip and the sample [34]. However, instead of the current as the controlling parameter, the electrostatic force is used. As the cantilever of an AFM is a very sensitive force probe, this technique results in a high sensitivity of

the CPD measurement, even for the very reduced size of the capacitor formed by the tip and the sample.

In addition to the compensation dc-voltage (V_{dc}) between tip and sample, an ac-voltage $V_{ac}\sin(\omega_{ac}t)$ at the frequency ω_{ac} is applied. The resulting oscillating electrostatic force induces an oscillation of the cantilever at the frequency ω_{ac}. Considering the tip-sample system as a capacitor, the electrostatic force in (2.8) can now be expressed as:

$$F_{el} = -\frac{1}{2}\frac{\partial C}{\partial z}[V_{dc} - V_{CPD} + V_{ac}\sin(\omega_{ac}t)]^2, \tag{2.12}$$

where $\partial C/\partial z$ is the capacitance gradient of the tip-sample system and the CPD is the difference in work function Φ between sample and tip:

$$V_{CPD} = \frac{\Delta\Phi}{e} = \frac{(\Phi_{sample} - \Phi_{tip})}{e}, \tag{2.13}$$

where e is the elementary charge.[1]

Equation (2.12) can be written as $F_{el} = F_{dc} + F_{\omega_{ac}} + F_{2\omega_{ac}}$, where the spectral components are:

$$F_{dc} = -\frac{\partial C}{\partial z}\left[\frac{1}{2}(V_{dc} - V_{CPD})^2 + \frac{V_{ac}^2}{4}\right], \tag{2.14}$$

$$F_{\omega_{ac}} = -\frac{\partial C}{\partial z}(V_{dc} - V_{CPD})V_{ac}\sin(\omega_{ac}t), \tag{2.15}$$

$$F_{2\omega_{ac}} = \frac{\partial C}{\partial z}\frac{V_{ac}^2}{4}\cos(2\omega_{ac}t). \tag{2.16}$$

Here, F_{dc} contributes to the topography signal, $F_{\omega_{ac}}$ at the ac-frequency is used to measure the CPD and $F_{2\omega_{ac}}$ can be used for capacitance microscopy (see Sect. 2.8) [14].

While the KPFM measurement results in the determination of the CPD, which is the work function of the sample relative to that of the tip, (2.13) can be used to deduce the sample's work function on an absolute scale. Using a calibrated tip with a known work function, the work function of the sample can be calculated from the CPD measurement according to (2.13). However, for absolute work function

[1] In principle, the definition of the CPD could also be selected as $V_{CPD} = (\Phi_{tip} - \Phi_{sample})/e$, which corresponds to $-V_{CPD}$ of (2.13). We selected the definition of (2.13) such that the changes in V_{CPD} directly correspond to changes in the work function. Thus, images of V_{CPD} represent the same contrast as images of the sample's work function Φ_{sample}, just with a constant absolute offset, which is equal to the work function of the tip. In the experimental realization this would correspond to a situation, where the voltage is applied to the sample and the tip is grounded (see Sect. 2.7).

measurements, operation under ultrahigh vacuum (UHV) conditions is mandatory [18], as it is well known that the work function is highly sensitive to the surface cleanness [23].

As in the case of the topography measurement, also for the CPD measurement two different modes can be distinguished. The amplitude modulation technique (AM-mode) controls the applied dc-bias by reducing the amplitude of the induced oscillation at the ac-frequency to zero, and the frequency modulation technique (FM-mode) minimizes the variation in the frequency shift Δf_0 at the ac-frequency.

2.4 AM-KPFM

In the AM-mode, the amplitude of the cantilever oscillation at the ac-frequency ω_{ac} is measured; it is induced by the electrostatic force and is proportional to this. The amplitude is detected using the beam deflection signal and a lock-in amplifier tuned to the frequency of the ac-bias (see also Sect. 2.7). As can be seen from (2.15), this signal is minimized by controlling V_{dc} to match the CPD V_{CPD}. Recording V_{dc} while scanning the topography, an image of the CPD is obtained. Many KPFM systems use this technique with ac-frequencies of several kHz to several tens of kHz. To get sufficient sensitivity, ac-voltages of 1–3 V are typically used [29, 30].

An improvement to this technique is obtained by tuning the ac-frequency to a resonance frequency of the cantilever. In this way a resonance-enhanced detection is achieved, providing the possibility to lower the ac-voltage maintaining a high sensitivity to the electrostatic force. Frequently, this is realized in the two-pass mode, where in the first scan-line the topography is determined, which is then retraced with the tip lifted up by several tens of nm, while an ac-voltage at the fundamental resonance frequency is applied for KPFM detection of V_{CPD}. This mode is described in more detail in Sect. 2.8 below. A more elegant way to use resonance-enhanced KPFM is to tune the ac-frequency to the second oscillation mode of the cantilever [19, 31]. While the fundamental resonance is mechanically excited and used for topography detection, the ac-voltage simultaneously excites electrostatically a cantilever oscillation, for example of the second oscillation mode, which is used for the CPD detection. Then the oscillation at ω_{ac} is amplified by the quality factor Q. This enhances the sensitivity and permits to use lower ac-voltages, down to the order of 100 mV. Working with the resonance-enhanced detection, also the response time of the system is determined by the quality factor. This can be quantitatively expressed in a similar way as for the fundamental resonance used for the topography detection [2]. The system reacts to a change (for example a change in the CPD upon scanning the tip) with a response time τ until a new stable state is reached, where [2, 16]:

$$\tau = \frac{Q}{\pi f_2}. \tag{2.17}$$

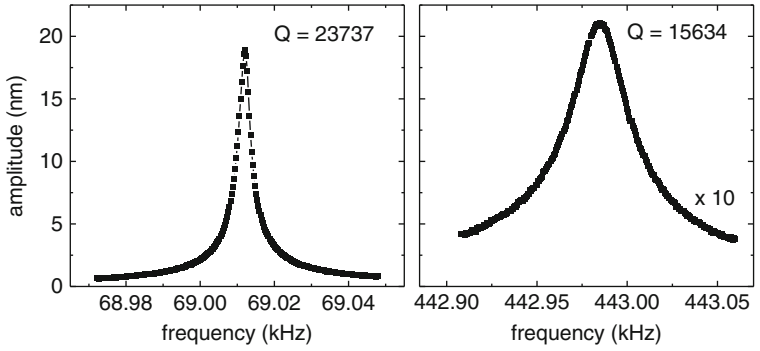

Fig. 2.3 Resonance peaks of the fundamental and second oscillation mode of a typical cantilever for force modulation AFM (Nanosensors PPP-EFM). The Q-factors for the two resonances are also given

Using typical values of $Q = 15,000$ and $f_2 = 450\,\text{kHz}$ the response time results to $\tau \approx 11\,\text{ms}$. This means that scanning is easily possible with scan speeds on the order of 1 s/line.

The limiting factor in this mode is the bandwidth of the photodiode used for the detection of the cantilever oscillation. This depends on the specific type and manufacturer of the AFM system. In many commercial systems a photodiode with a bandwidth of $\sim$500 kHz is used; therefore, the stiffest cantilevers used for detection on the second oscillation mode have the fundamental resonance frequency in the range of 70–80 kHz, and the second resonance around 400–470 kHz ($f_2 \sim 6.3 f_0$, due to the geometry of the cantilever [5]). Typical resonance curves for the fundamental and second oscillation mode are shown in Fig. 2.3. The amplitude of the second resonance mode is smaller by about a factor of 10 when the same excitation amplitude is used for the mechanical excitation of the dither-piezo.

Thus, the resonance-enhanced AM-mode KPFM has two advantages: (1) a simultaneous measurement of topography and CPD is possible due to the use of two independent resonance modes and (2) the resonance enhancement provides a higher sensitivity to the electrostatic force and therefore allows to use smaller ac-voltages. This in turn has two additional advantages. First, the ac-amplitude affects the topography image by inducing a constant electrostatic background, as can be seen by the $V_{\text{ac}}^2/4$-term in (2.14). Second, large ac-voltages possibly induce band bending at the surface of semiconductors [33], which would cause an incorrect determination of the work function.

2.5 FM-KPFM

In the frequency modulation mode, the applied ac-bias voltage induces a modulation of the electrostatic force, which results in an oscillation of the frequency shift Δf_0 at the frequency ω_{ac} of the ac-bias. This oscillation is detected by a lock-in amplifier

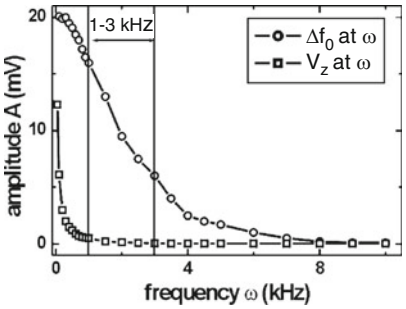

Fig. 2.4 Dependence of the frequency shift Δf_0 and the height control signal of the topography V_z at the frequency ω of the ac-voltage. The measurements were obtained on a HOPG sample with a bias slightly above the CPD using a room temperature UHV-AFM system by Omicron nanotechnology [12]

tuned to the frequency of the ac-bias. The measured signal is approximately proportional to the force gradient, as can be concluded from (2.10) and (2.15):

$$\Delta f_0(\omega_{\mathrm{ac}}) \propto \frac{\partial F_{\omega_{\mathrm{ac}}}}{\partial z} = \frac{\partial^2 C}{\partial z^2}(V_{\mathrm{dc}} - V_{\mathrm{CPD}})V_{\mathrm{ac}}\sin(\omega_{\mathrm{ac}}t). \tag{2.18}$$

As was shown in [12], the frequency ω_{ac} has to be chosen in an appropriate range. The lower limit is dictated by an increasing cross talk to the topography signal: if the frequency is too low, the tip-sample distance control follows the additional electrostatic force and the tip-sample distance starts to oscillate at the frequency ω_{ac}. The higher the frequency the lower the coupling to the topography. On the other hand, the bandwidth of the frequency demodulator or the PLL determines the upper limit of the frequency range. Figure 2.4 shows the amplitudes at ω_{ac} of the oscillation of Δf_0 and of the oscillation of the piezo-voltage V_z, which controls the tip-sample distance. With increasing frequency ω_{ac} the cross talk to the topography signal decreases but also the signal intensity of the electrostatic force decreases due to the restricted bandwidth of the frequency demodulator. Also in this mode, higher V_{ac} results in higher sensitivity at the cost of an influence on the topography and a possibly induced band bending on semiconductor samples (see above). Typical values for $f_{\mathrm{ac}} = \omega_{\mathrm{ac}}/2\pi$ and V_{ac} are in the range of 1–3 kHz and 1–3 V, respectively.

2.6 Comparison of AM- and FM-KPFM

As was shown in the previous two chapters, the AM-mode KPFM is sensitive to the electrostatic force, whereas the FM-mode is sensitive to the electrostatic force gradient. As a result of this difference, also different properties of the two modes can

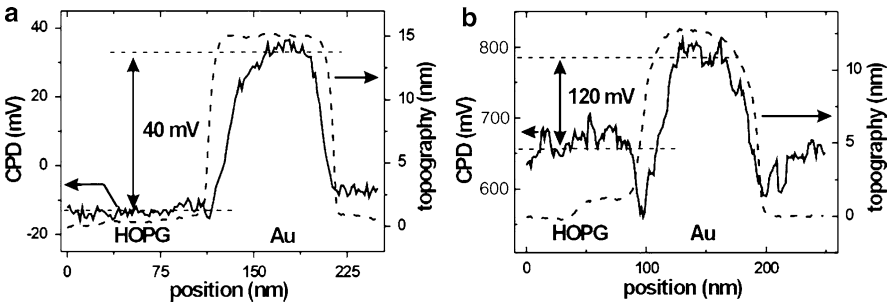

Fig. 2.5 AM- and FM-mode measurements on a HOPG sample with Au islands. Single line profiles are shown for the topography (*dashed lines*) and CPD (*solid lines*) in (**a**) AM-mode and (**b**) FM-mode KPFM. The AM-mode was conducted with a cantilever with force constant $\sim 3\,\mathrm{N\,m^{-1}}$ and the FM-mode with a stiffer cantilever of $\sim 42\,\mathrm{N\,m^{-1}}$ [12]

be expected in KPFM measurements. Especially the spatial and energy resolution can be different, as will be shown in this section.

The first concise study for the comparison of AM- and FM-KPFM was presented by Glatzel et al. [12]. In this experimental study, the authors used dendritic gold islands on highly oriented pyrolytic graphite (HOPG) as a model system so study the spatial and energy resolution in both operation modes. As can be seen in Fig. 2.5, the difference in CPD between graphite and gold amounts to about 40 meV in the AM-mode and about 120 meV in the FM-mode. As the gold island size is on the order of $\sim$100 nm, the large difference is explained by the fact that in the AM-mode, the tip averages over a larger area on the sample, where more of the surrounding gold islands and graphit substrate are "seen" by the tip due to the longe-range nature of the electrostatic force; this leads to a measurement of an averaged CPD value for Au and graphite. In contrast, the difference in CPD between gold and graphite is about 3 times larger in the FM-mode. The relevant force gradient in this mode is much more short-ranged and therefore averaging takes place over a much smaller area below the tip. Thus, the tip mainly "sees" only the confined area right below the tip. This also affects the spatial resolution [12], as is also visible in Fig. 2.5.

A subsequent study by Zerweck et al. [37] presented a comparison between AM- and FM-KPFM by experiments on KCl islands deposited on a Au(111) substrate. In addition, the authors also performed three dimensional (3D) finite element simulations describing the electrostatic field between the metallic tip and the sample surface. Thereby, a comparison between experimental and simulation result became possible. In the simulations the tip is modeled as a truncated cone merging into a half sphere with radius R opposed to a circular surface representing the sample. The cantilever is described as a disk at the base of the cone. For the simulation of the spatial resolution, the sample consists of two halves, one at negative and the other at positive potential. For this model, the electric field distribution was calculated for different potential differences V between tip and sample. The electric field energy

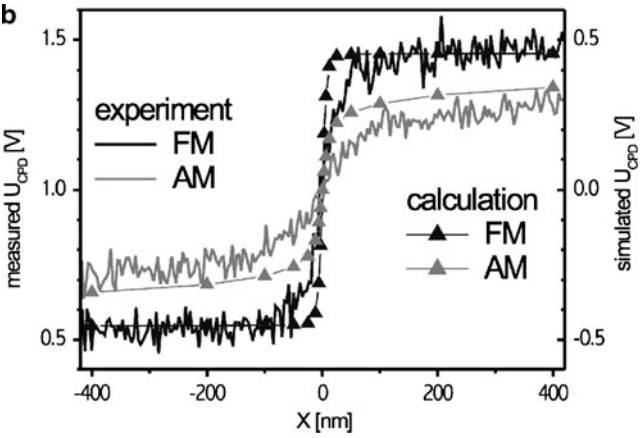

Fig. 2.6 Experimental line profiles (*solid lines*) extracted from KPFM images of a KCl island (*left half*) on a Au substrate (*right half*) recorded in AM- (*gray*) and FM-mode (*black*). The simulation of the two modes is shown as the *triangular* symbols and provides a good description of the experimental data. For the simulation, a potential difference of 0.9 V between the two regions was assumed [37]

was then obtained by integration of the square of the electric field. Differentiation of the electric field energy with respect to the vertical direction then gives the electrostatic force $F_{\mathrm{el}}(z, V)$ acting normal to the surface and further differentiation results in the electrostatic force gradient $\partial F_{\mathrm{el}}(z, V)/\partial z$ [37]. For a fixed separation and lateral position, both F_{el} and $\partial F_{\mathrm{el}}/\partial z$ depend on V. Consequently, the CPD for the AM-KPFM corresponds to the minimum of $F_{\mathrm{el}}(z, V)$, and the CPD for FM-KPFM to that of $\partial F_{\mathrm{el}}(z, V)/\partial z$.

Figure 2.6 shows a comparison of experimental data obtained in AM- and FM-mode on a sample consisting of KCl islands on a Au(111) substrate and a simulation of both modes [37]. As can be seen, the energy resolution is considerably better in the FM-mode, which reaches the expected CPD difference between KCl and Au within about 50 nm of the transition. For the AM-mode, the full CPD difference is not even reached within 400 nm of the transition, showing clearly that the spatial resolution of the transition is much better in the FM-mode. Additionally, the authors evaluated the dependence of the energy resolution on the tip-sample separation, finding that for separations up to about 30 nm the FM-mode gives an excellent agreement between experiment and simulation. For larger tip-sample distances the force gradient becomes too small and the controller becomes unstable. For the AM-mode a large deviation from the expected CPD values is found for all distances considered in the study [37]. Therefore, it is recommended to maintain a tip-sample distance as small as possible. It has to be mentioned that in the experiments and simulations of [37] the regular AM-mode was considered. Thus the results are not directly comparable to the resonance-enhanced AM-mode KPFM, where the ac-frequency is applied at the second oscillation mode, as used in the experimental study of [12].

2.7 Technical Realization

Figure 2.7 shows a typical setup of the electronic system of a KPFM. The cantilever oscillation is detected by a beam deflection method using a laser, reflected from the backside of the cantilever onto a position sensitive photo diode. The signal is fed into a frequency detector, as for example a PLL or a frequency demodulator, which mechanically excites the cantilever oscillation on the fundamental resonance frequency. A frequency generator feeds the desired ac-voltage into an adder element, and at the same time provides the reference frequency for the lock-in amplifier. Depending on the used lock-in amplifier, also the reference output voltage can be used directly as the ac-bias for the sample. In FM-mode KPFM, the signal from the frequency detector is directly fed into the Lock-In amplifier (see dashed arrow in Fig. 2.7), which then detects the magnitude of the frequency shift at the ac-frequency, induced by the resulting additional electrostatic forces. The lock-in output serves as input to the Kelvin-controller, which adjusts a dc-voltage such that the input signal (S) goes toward zero. This dc-voltage is the second input to the adder, which provides then the complete voltage to the sample, consisting of the sum of ac- and dc-bias. On the other hand, as was shown above, the dc-bias matches the CPD and thus the dc-bias is recorded with the scan, to provide the spatially resolved CPD image.

Figure 2.7 shows also the setup for the AM-mode KPFM. In this case, the output signal from the position sensitive photodiode is passed not only to the FM-demodulator, but additionally to the input of the lock-in amplifier, as shown

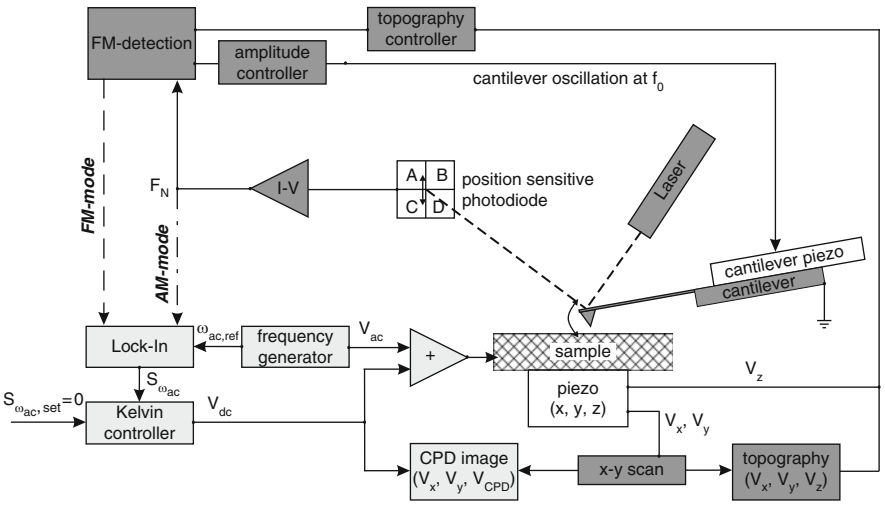

Fig. 2.7 Block diagram of the electronic realization of a KPFM. The *dashed line* indicates the FM-mode and the *dashed-dotted line* the AM-mode setup. *Dark grey boxes* are the regular non-contact AFM topography part and the *light gray boxes* are the KPFM part of the setup. See text for details

by the dashed-dotted arrow in Fig. 2.7. The rest of the setup is identical to the FM-mode setup. Thus, in the AM-mode, the amplitude of the induced oscillation of the cantilever is measured directly, as described above in Sect. 2.4. For a better separation of the fundamental resonance frequency from the ac-frequency signal from the photo diode a high and/or low-pass filter might optionally by used.

2.8 Other Modes and Additional Experimental Options

As described above, the KPFM uses a controller to compensate the electrostatic forces between the AFM-tip and the sample by applying a dc-bias which matches the CPD. The signal which is fed into the controller is the output of a lock-in amplifier (see Fig. 2.7). This lock-in measures the magnitude of the electrostatic forces induced by the applied ac-voltage. Instead of compensating the electrostatic forces through application of the dc-bias by the controller, one can also directly image the electrostatic forces by recording the magnitude of the lock-in signal. This measurement mode is called electrostatic force microscopy (EFM) and provides the advantage of a possibly higher imaging speed, as the additional Kelvin-controller is avoided. For getting reasonable signal-to-noise ratios, the Kelvin controller time constant is usually kept on the order of several ms up to several tens of ms, reducing the scan speed to the order of a few seconds per scan line. On the other hand, a clear disadvantage of the EFM is the lack of a quantitative measurement of the CPD. The EFM signal gives only access to relative changes in the CPD, however, the KPFM provides a quantitative measure of the CPD. Nevertheless, the literature reports many EFM studies, likely motivated by the fact, that experimentally the EFM technique is simpler to handle and requires less equipment, namely it does not require a Kelvin controller.

The capability of KPFM to acquire images of the CPD relies on (2.15), as discussed above. A closer examination of (2.15) shows that the electrostatic force component at the ac-frequency ω_{ac} not only exhibits the dependence on the voltage difference $(V_{dc} - V_{CPD})$, but also a possible contribution from the capacitance gradient $\partial C/\partial z$ has to be considered. Local variations of this contribution possibly affect measurements. This effect should be severe for EFM imaging, where the CPD is not compensated and therefore variations in the EFM signal obtained from the lock-in amplifier might erroneously be attributed to CPD variations. However, the effect on KPFM images should be much smaller or even negligible, as the Kelvin-controller reduces the $(V_{dc} - V_{CPD})$ part of (2.15) to zero. Therefore the $\partial C/\partial z$ contribution should not affect KPFM imaging. Moreover, considering (2.16), it is seen that by monitoring the induced oscillation of the cantilever at the frequency $2\omega_{ac}$ it becomes possible to acquire an image of $\partial C/\partial z$ [1, 21]. In the case of applying the FM-mode imaging, the corresponding second derivative would be imaged: $\partial C^2/\partial^2 z$. As (2.16) is independent of the applied dc-bias V_{dc} and V_{CPD}, the only dependence of this force component stems from variations in the capacitance

gradient. In the experimental set-up, such a measurement can be realized by using an additional lock-in amplifier with the reference tuned to $2\omega_{ac}$, which then as an output signal provides the capacitance gradient [14].

Hochwitz et al. [14] have used this capacitance imaging to study complementary metal-oxide-semiconductor (CMOS) gates. Comparing individual devices in a CMOS chip, the monitored CPD did not show a clear distinction between properly functioning gates and gates that failed in operation. However, the capacitance gradient provided a clear signal difference between functional and non-functional CMOS gates. The authors concluded therefore, that the mechanism for the failure is beneath the surface. While the KPFM imaging is highly surface sensitive, the capacitance gradient provides also information from a region below the surface.

The subsurface sensitivity of the capacitance imaging is explained by the fact that for semiconductors the application of the ac-bias V_{ac} affects the charge distribution at the surface and subsurface region below the tip. Depending on the doping type of the sample and whether the ac-bias is in the positive or negative half of the oscillation cycle, the surface will undergo accumulation or depletion, respectively. The magnitude of the resulting change in the capacitance gradient depends on the charge carrier concentration [22, 25], similar to the way scanning capacitance microscopy works [35].

It was described above, that the sensitivity of KPFM can be enhanced by tuning the ac-frequency to a resonance of the cantilever and therefore obtain a resonance enhanced detection of the CPD. When using the second resonance mode for the ac-frequency, the simultaneous measurement of topography and CPD becomes possible (see above). However, frequently a two-pass method of KPFM is used. In this operation mode, the sample topography is scanned in either non-contact or in TappingMode™ and then in a second scan across the same line, this topography is retraced with the tip being retracted from the surface and the mechanical cantilever oscillation switched off. For the retrace the tip is usually lifted a few tens of nm away from the surface. The ac-bias for the KPFM measurement can now be applied at the fundamental resonance frequency and thus allow a resonance enhanced detection of the electrostatic forces and their compensation by the Kelvin-controller [25]. While the resonance-enhanced detection presents advantages for the sensitivity of the KPFM measurement, several problems with this technique have to be considered. (1) In the case of piezo creep or thermal drift, the retraced topography profile might not exactly match the topography right beneath the tip and therefore the exact tip-sample distance is not known during the Kelvin scan. (2) The larger tip-sample distance due to the lifted tip results in a lower resolution of the KPFM image, due to the resulting larger averaging effect. (3) The measurement of the topography is subject to electrostatic forces due to local CPD differences, which results in an incorrect determination of the sample topography during the first scan [27, 36]. When using the two-pass method for KPFM, all these effects will influence the CPD image. Therefore, care has to be taken when data are analyzed, especially when small details are considered, or when CPD contrast is related to changes in the sample topography.

2.9 Additional Remarks

Due to the extremely short-range nature of the tunneling current, an STM provides a high sensitivity to the sample topography; the tunneling current passes almost exclusively through the outer-most tip atom. In contrast to this, in KPFM the electrostatic forces are relevant for the imaging process. Since those have a long-range character, it is not anymore the outer-most tip atom, but the whole tip, which determines the interaction between tip and sample, possibly also the cantilever itself. Therefore, the tip shape plays a role in KPFM imaging and several authors have studied the influences. Colchero et al. [6] have analytically investigated the influence of the tip and the cantilever in EFM. Based on their analysis, the cantilever plays an important role in EFM and AM-KPFM imaging, despite the fact that the distance between cantilever and sample is $\sim 10^4$ times larger than the distance between the tip apex and the sample. However, due to the much larger surface area of the cantilever with respect to the tip apex, its role remains important. Their suggestion to avoid a reduction in spatial resolution due to interaction with the cantilever is to use the FM-KPFM. Due to the shorter interaction range of the force gradient, the influence of the cantilever is considerably reduced, providing for a good spatial resolution. This was later confirmed quantitatively by Zerweck et al. [37], who performed finite element simulations to describe the electrostatic interaction between the tip and a sample and extract the spatial resolution from scan lines of model structures (see Sect. 2.5). Basically, the resolution in FM-mode imaging is limited by the tip radius [28]. However, both studies did not consider the resonance-enhanced AM-mode KPFM, which in many experimental studies has also provided very high resolution on the order of the tip radius [26, 32], even down to the atomic scale [9].

The influence of the cantilever on EFM and KPFM imaging was also studied by investigating the dependence of the relative contribution of the capacitance derivative for the tip and the cantilever. Hochwitz et al. [13] numerically simulated the influence of the tip-to-cantilever area and the relative tip-to-cantilever distance to the sample on the ratio $\left(\partial C_{\mathrm{tip}}/\partial z\right) / \left(\partial C_{\mathrm{cantilever}}/\partial z\right)$. The relative area of the cantilever to the tip was varied between 10^1 and 10^9 and the ratio between the tip-sample distance and the cantilever-sample distance was varied between 10^{-1} and 10^{-4}. As is shown in Fig. 2.8, the ratio of tip to cantilever capacitance gradient varies in form of a relatively sharp step function. The authors find an optimal working region for KPFM or EFM with the cantilever to tip area in the range between 10^3 and 10^6 and the tip-sample distance to cantilever-sample distance to be less than 10^{-3}. This last criterium means that for a typical tip height of $\sim 10\,\mu\mathrm{m}$ a tip-sample distance of 10 nm or less should be maintained. On the other hand, the first criterium leads to the conclusion, that the intuitive guess that a finer tip results in a finer resolution only applies to a certain limit. If the tip gets too sharp, a decrease in resolution results, since the ratio of cantilever area to tip area increases. Thus, long, slender and slightly blunt tips should provide better resolution [13].

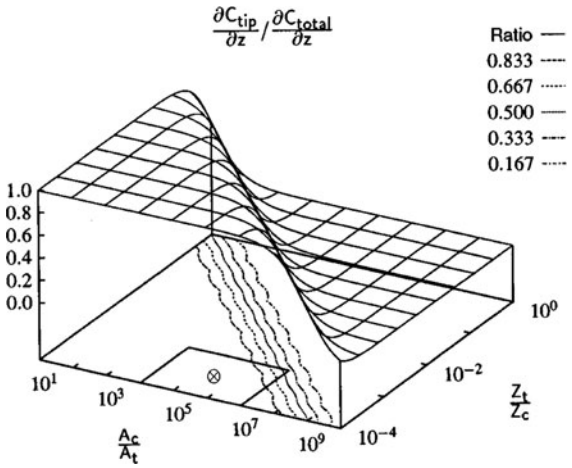

Fig. 2.8 Surface plot showing the relative contribution of the tip/sample capacitance compared to the total probe/sample capacitance as functions of the area and sample spacing over a topographically flat surface. A_c/A_t is the ratio of the cantilever area to the tip area and Z_t/Z_c is the ratio of the tip/sample distance to the cantilever/sample distance [13]

An experimental study confirming the simulations of Hochwitz et al. [13] was presented by Glatzel et al. [12]. Different cantilever types were comparatively used for the imaging of gold islands on a HOPG substrate. For the nominally same tip radius, short tips provide less potential contrast between Au and HOPG as compared to measurements with tips with a 3–5 times larger tip height. For the latter tips, the cantilever is further away from the sample and therefore the averaging due to the long-range electrostatic force is reduced. Experimentally, the CPD contrast between gold and graphite was about twice as large for the longer tips.

Sadewasser and Lux-Steiner [27] showed the impact of the electrostatic forces on the topography imaging with regular nc-AFM imaging at fixed sample bias. For a fixed sample bias the electrostatic force acting on the tip is different depending on the local CPD under the present tip position, as can be seen from (2.12). Thus, these uncompensated electrostatic forces contribute to the topography contrast, in addition to the van-der-Waals forces. For a sample consisting of only two materials with different CPD, correct topography imaging is possible, when the sample bias is selected to correspond to the average CPD of the two materials. However, for more than two materials, it is not possible to apply a fixed bias and maintain a correct imaging of the topographic structure in nc-AFM [27]. In such a case, KPFM has to be used to provide a local compensation of the electrostatic forces and allow imaging of the topography based on purely van der Waals forces. These conclusions apply to KPFM imaging in the AM- as well as in the FM-mode. Thus, KPFM not only allows imaging the CPD structure of a sample, but also provides for a topography imaging free from the influence of electrostatic forces. The relevance of electrostatic forces for topography imaging in nc-AFM was also addressed by Dianoux et al. [8].

References

1. D.W. Abraham, C. Williams, J. Slinkman, H.K. Wickramasinghe, J. Vac. Sci. Technol. B **9**, 703 (1991)
2. T.R. Albrecht, P. Grütter, D. Horne, D. Rugar, J. Appl. Phys. **69**, 668 (1991)
3. G. Binnig, H. Rohrer, Ch. Gerber, E. Weibel, Phys. Rev. Lett. **49**, 57 (1982)
4. G. Binnig, C.F. Quate, Ch. Gerber, Phys. Rev. Lett. **56**, 930 (1986)
5. H.-J. Butt, M. Jaschke, Nanotechnology **6**, 1 (1995)
6. J. Colchero, A. Gil, A.M. Baró, Phys. Rev. B **64**, 245403 (2001)
7. B.V. Derjaguin, V.M. Muller, Y.P. Toporov, J. Colloid. Interf. Sci. **53**, 314 (1975)
8. R. Dianoux, F. Martins, F. Marchi, C. Alandi, F. Comin, J. Chevrier, Phys. Rev. B **68**, 045403 (2003)
9. G.H. Enevoldsen, Th. Glatzel, M.C. Christensen, J.V. Lauritsen, F. Besenbacher, Phys. Rev. Lett. **100**, 236104 (2008)
10. R. García, R. Pérez, Surf. Sci. Rep. **47**, 197 (2002)
11. F.J. Giessibl, Phys. Rev. B **56**, 16010 (1997)
12. Th. Glatzel, S. Sadewasser, M.Ch. Lux-Steiner, Appl. Sur. Sci. **210**, 84 (2003)
13. T. Hochwitz, A.K. Henning, C. Levey, C. Daghlian, J. Slinkman, J. Vac. Sci. Technol. B **14**, 457 (1996)
14. T. Hochwitz, A.K. Henning, C. Levey, C. Daghlian, J. Slinkman, J. Never, P. Kaszuba, R. Gluck, R. Wells, J. Pekarik, R. Finch, J. Vac. Sci. Technol. B **14**, 440 (1996)
15. J.N. Israelachvili, *Intermolecular and Surface Forces* (Academic, London, 1992)
16. S. Kawai, H. Kawakatsu, Appl. Phys. Lett **89**, 013108 (2006)
17. L. Kelvin, Phil. Mag. **46**, 82 (1898)
18. A. Kikukawa, S. Hosaka, R. Imura, Appl. Phys. Lett. **66**, 3510 (1995)
19. A. Kikukawa, S. Hosaka, R. Imura, Rev. Sci. Instrum. **67**, 1463 (1996)
20. Y. Martin, C.C. Williams, H.K. Wickramasinghe, J. Appl. Phys. **61**, 4723 (1987)
21. Y. Martin, D.W. Abraham, H.K. Wickramasinghe, Appl. Phys. Lett. **52**, 1103 (1988)
22. F. Müller, A.-D. Müller, M. Hietschold, S. Kämmer, Meas. Sci. Technol. **9**, 734 (1998)
23. M. Nonnenmacher, M.P. O'Boyle, H.K. Wickramasinghe, Appl. Phys. Lett. **58**, 2921 (1991)
24. R. Pérez, M.C. Payne, I. Stich, K. Terukura, Phys. Rev. Lett. **78**, 678 (1997)
25. P.A. Rosenthal, E.T. Yu, R.L. Pierson, P.J. Zampardi, J. Appl. Phys. **87**, 1937 (1999)
26. Y. Rosenwaks, R. Shikler, Th. Glatzel, S. Sadewasser, Phys. Rev. B **70**, 085320 (2004)
27. S. Sadewasser, M.Ch. Lux-Steiner, Phys. Rev. Lett. **91**, 266101 (2003)
28. K. Sajewicz, F. Krok, J. Konior, Jpn. J. Appl. Phys. **49**, 025201 (2010)
29. R. Shikler, T. Meoded, N. Fried, Y. Rosenwaks, Appl. Phys. Lett. **74**, 2972 (1999)
30. R. Shikler, T. Meoded, N. Fried, B. Mishori, Y. Rosenwaks, J. Appl. Phys. **86**, 107 (1999)
31. Ch. Sommerhalter, Dissertation, Freie Universität Berlin (1999)
32. Ch. Sommerhalter, Th.W. Matthes, Th. Glatzel, A. Jäger-Waldau, M.Ch. Lux-Steiner, Appl. Phys. Lett. **75**, 286 (1999)
33. Ch. Sommerhalter, Th. Glatzel, Th.W. Matthes, A. Jäger-Waldau, M.Ch. Lux-Steiner, Appl. Surf. Sci. **157**, 263 (2000)
34. J.M.R. Weaver, D.W. Abraham, J. Vac. Sci. Technol. B **9**, 1559 (1991)
35. C.C. Williams, Annu. Rev. Mater. Sci. **29**, 471 (1999)
36. M. Yan, G.H. Bernstein, Ultramicroscopy **106**, 582 (2006)
37. U. Zerweck, Ch. Loppacher, T. Otto, S. Grafström, L.M. Eng, Phys. Rev. B **71**, 125424 (2005)
38. L. Zitzler, S. Herminghaus, F. Mugele, Phys. Rev. B **66**, 155436 (2002)